Deep Corneal Nerve Plexus Selective Damage in Persistent Neurotrophic Corneal Epithelial Defects Detected by In Vivo Multiphoton Confocal Microscopy

Seitaro Komai,[1,2] Manuel E. Quiroga-Garza,[1,2] Raul E. Ruiz-Lozano,[1,2] Nadim S. Azar,[1,2] Hazem M. Mousa,[1] Sofia Murillo,[1] Symon Ma,[1,2] Ali Khodor,[2] Sejiro Littleton,[1,3] Daniel R. Saban,[1–3] Alain Chédotal,[4–6] and Victor L. Perez[1,2]

[1]Foster Center for Ocular Immunology, Duke Eye Center, Department of Ophthalmology, Duke University School of Medicine, Durham, North Carolina, United States
[2]Bascom Palmer Eye Institute, University of Miami, Miami, Florida, United States
[3]Department of Immunology, Duke University School of Medicine, Durham, North Carolina, United States
[4]Institut de la Vision, Sorbonne Université, INSERM, CNRS, Paris, France
[5]Institut de pathologie, groupe hospitalier Est, hospices civils de Lyon, Lyon, France
[6]MeLiS, CNRS UMR5284, Inserm U1314, University Claude Bernard Lyon 1, Lyon, France

Correspondence: Victor L. Perez, Bascom Palmer Eye Institute, University of Miami Miller School of Medicine, McKnight Vision Research Center, 900 NW 17th St., Miami, FL 33136, USA; vperez4@med.miami.edu.

Received: September 1, 2024
Accepted: January 24, 2025
Published: April 1, 2025

Citation: Komai S, Quiroga-Garza ME, Ruiz-Lozano RE, et al. Deep corneal nerve plexus selective damage in persistent neurotrophic corneal epithelial defects detected by in vivo multiphoton confocal microscopy. *Invest Ophthalmol Vis Sci.* 2025;66(4):1. https://doi.org/10.1167/iovs.66.4.1

Purpose. To investigate the corneal nerve damage in neurotrophic corneal persistent epithelial defects by an in vivo imaging system using in vivo multiphoton confocal microscopy (MCM) and calcitonin gene-related peptide (CGRP):GFP Tg mice.

Methods. Corneal epithelium was scraped, followed by administering a single dose of benzalkonium chloride (BAK) to develop a neurotrophic persistent epithelial defect. The defect was imaged with fluorescein staining for up to 24 hours, and wound closure percentage (%, WCP) was calculated. CGRP:GFP Tg mice were used in combination with in vivo MCM to acquire in vivo images of corneal nerve before and 24 hours after the creation of a corneal epithelial defect. GFP signals from CGRP-positive nerves were reconstructed into three-dimensional (3D) images, and nerve volume was analyzed. Additionally, corneal mechanosensation was evaluated using Cochet–Bonnet esthesiometry.

Results. BAK-treated eyes showed a significant delay in WCP at 24 hours. In CGRP:GFP Tg mice, CGRP-positive nerves were successfully captured by in vivo MCM and reconstructed into 3D images. BAK-treated eyes showed a significant decrease in both stromal nerve volume and corneal mechanosensation compared to no BAK eyes at 24 hours after corneal scraping, suggesting that BAK impaired the stromal nerves in both structural and functional asides.

Conclusions. Our in vivo corneal nerve imaging system using the combination of in vivo MCM and CGRP:GFP Tg mice demonstrated a longitudinal observation of murine corneal nerves. This system revealed that corneal stromal nerves were selectively damaged in persistent neurotrophic corneal epithelial defects and offered outstanding potential for various applications.

Keywords: corneal nerves, corneal epithelial wound healing, in vivo nerve imaging, in vivo confocal microscopy

The corneal epithelium plays a crucial role as a barrier, preventing the entry of microorganisms and fluids from entering the eye. Consequently, the cornea depends on a high wound-healing rate to repair epithelial defects. However, certain comorbidities may affect the cornea's repair capabilities, increasing the risk of persistent epithelial defects (PEDs), which, if left unaddressed, can have severe consequences such as infection and vision loss.[1,2] Management of PEDs is complex and involves a wide spectrum of treatments, ranging from topical anti-inflammatory medications, amniotic membrane grafts, autologous serum tears, and whole blood-derived products. More invasive approaches, such as conjunctival flaps, corneal neurotization, and even penetrating keratoplasty, may be necessary when perforation is imminent.[3–6] The corneal epithelium is one of the most densely innervated tissues in the human body, receiving branches from the V_1/ophthalmic division of the trigeminal nerve.[7] Corneal nerves play a significant role in the corneal epithelial wound-healing process, and compromise of corneal nerve integrity is associated with PEDs.[1] Previous studies on corneal epithelial wound healing have led to the development of murine models that replicate this condition. However, these models are designed in the context of other specific pathologic backgrounds

like diabetes mellitus.[8–11] In contrast, neuropathic PEDs can develop in healthy individuals as a result of certain topical medications or physical damage to the corneal nerves. For example, the antimicrobial compound benzalkonium chloride (BAK), a common preservative in eye drop formulations, can cause neurotrophic PEDs[12,13] and delayed corneal wound healing[14–16] due to its notable impact on the corneal epithelial surface[17–23] as well as corneal nerves.[24–28]

From the perspective that the corneal nerves are involved in maintaining corneal epithelia, it is imperative to assess the pathogenesis of delayed corneal wound healing from both an epithelial and a neural perspective. Traditional analysis of corneal innervation in animal models relies on whole-mount sections of the cornea and immunostaining for neural markers such as β-III-tubulin and PGP-9.5, receptors like transient receptor potential vanilloid 1 (TRPV1), and neuropeptides like substance P and calcitonin gene-related peptide (CGRP).[9,10,29–32] However, this approach presents challenges, including the potential for incomplete staining due to insufficient penetration of the antibody throughout cornea.[33] In addition, the requirement for euthanasia precludes longitudinal observation of the corneal epithelium and nerves over time. Therefore, visualization of the corneal epithelium and nerve organization/patterning would greatly benefit from a noninvasive technique with in vivo longitudinal capabilities that does not depend solely on immunohistochemistry.

Current available methods for imaging corneal nerves in preclinical models include fluorescent microscopy, intravital confocal microscopy, transmission,[34] scanning,[35] and serial block face scanning electron microscopy.[36] CGRP is a neuropeptide and has previously been employed as a marker for labeling peptidergic sensory neurons and their terminals.[7,26] In the mouse cornea, CGRP is released from nociceptive C-fibers along with substance P, making it ideal for neuronal evaluation in rodent models, especially in those related to pain sensation.[33] With this understanding, Bouheraoua et al.[33] used a CGRP–green fluorescent protein (GFP) transgenic (Tg) mouse model to observe nerve distribution in the cornea. Notably, $CGRP^+$ nerves account for 56% to 64% of all β-III-tubulin$^+$ nerves in the central cornea. Given the critical role of CGRP neurons in pain perception pathways, the use of CGRP:GFP transgenic mice presents a unique opportunity to understand the pathophysiology of PEDs.

The combination of in vivo microscopy and fluorescent-labeled Tg mice allows noninvasive visualization of tissues without any need for antibodies or dyes. The in vivo imaging system of corneal nerves and dendritic cells using $CD11c^{YFP} \times Thy1^{YFP}$ Tg mice and multiphoton microscopy has been first reported to evaluate real-time interactions between nerves and conventional dendritic cells in the cornea.[37] In this study, a novel in vivo corneal nerve imaging system for corneal nerve mapping was developed using in vivo multiphoton confocal microscopy to image corneal nerves in CGRP:GFP Tg mice without euthanasia. Three-dimensional (3D) images of CGRP-positive corneal nerves were reconstructed, enabling 3D analysis of nerve morphology. Furthermore, this new in vivo imaging system of murine corneal nerves was successfully applied to a mouse model of delayed corneal epithelial wound healing induced by topical BAK administration to observe the morphology and distribution of corneal nerves at multiple time points, thereby demonstrating that BAK selectively damages the deep corneal nerve plexus. By acquiring longitudinal data, we propose that this approach provides a new method for evaluating corneal wound healing and corneal nerves.

Materials and Methods

Animals (C57/B6 and CGRP:GFP Tg Mice)

Bacterial artificial chromosome CGRP:GFP transgenic (Tg) mice (female, aged 8 to 10 weeks) were used to visualize CGRP-positive corneal nerve axons without immunostaining. In the CGRP:GFP Tg mouse construct, CGRP is labeled by downstream insertion of GFP in the *Calca* gene, which encodes CGRP.[33] Female 8- to 10-week-old C57/B6 mice (purchased from the Jackson Laboratory, Bar Harbor, ME, USA) were used in corneal epithelial wound-healing experiments. All animals were housed and handled at the Albert Eye Research Institute at Duke University (Durham, NC, USA) in compliance with the tenets of the ARVO Statement for the Use of Animals in Ophthalmic and Vision Research. Animal procedures were previously approved by Duke's Institutional Animal Care and Use Committee.

In Vivo Multiphoton Confocal Microscope Imaging and Acquisition of 3D Images of Corneal Nerves

CGRP:GFP Tg mice were anesthetized with an intraperitoneal injection of xylazine (10 mg/kg) and ketamine (100 mg/kg). To achieve adequate general anesthesia, we waited until eye movements were completely suppressed. The mouse's head was then secured in a three-point holder (one point on the teeth and two on the temporal head), carefully adjusting the holder's height and tilt to position the corneal apex directly toward the objective lens. Due to respiratory suppression from the anesthesia, head fixation minimized any eyeball vibration from residual breathing. This setup was inside a light-shielded box with a heater to maintain a stable body temperature of 37°C during the process. Then, 1 µL 0.3% hydroxypropyl methylcellulose (Ciba Vision, Duluth, GA, USA) was instilled on the ocular surface to prevent desiccation.

A Leica SP8 DIVE in vivo multiphoton confocal microscope (Leica Microsystems, GmbH, Wetzlar, Germany) was used for acquiring images composed of GFP fluorescence from $CGRP^+$ axons as well as second harmonic generation (SHG) from the corneal stroma matrix. Signals were obtained at a detection range of 490 to 560 nm for GFP and 455 to 470 nm for SHG with an excitation wavelength of 925 nm. GFP signals from $CGRP^+$ axons (green channel) and the second harmonic signals from the corneal stroma (blue channel) were obtained using a 16× objective lens. Then, 0.3% hydroxypropyl methylcellulose was placed between the lens and the corneal surface. A nine-tile Z-stack of coronal corneal images was acquired using LAS X software v.3.5.5 (Leica Microsystems, Bensheim, Germany). Each tile was 553.57 × 553.57 µm (512 × 512 pixels, with a 1.08-µm pixel size). Z-stacks ranged from 10 µm above the corneal apex to approximately 400 µm below. Z-stack interval was automatically determined by the LAS X software to be 1.63 µm. In addition, "line averaging" feature, which averages four images during imaging, was constantly used to compensate for movements caused by breathing and fine eye movements.

The Imaris software v.9.9.1 (Oxford Instruments Andor, Belfast, UK) was used to construct 3D image stacks and

to quantify the epithelial and stromal nerve volumes. First, each tile of the nine-tile *Z*-stacks was manually aligned using the application Imaris Stitcher v.9.9.1 (Oxford Instruments Andor). Afterward, a stromal volumetric surface was created using the *Surface* tool based on the SHG signal through the blue channel. The absolute intensity threshold was manually set for each Z-stack image, followed by automatic tracing and surface rendering.

GFP signal through the green channel was segmented depending on its intra- or extra-stromal location to visualize corneal nerves separately. To achieve this, the masking function was used on the rendered stroma volumetric surface. Briefly, the *Mask All* option was selected to eliminate the nerve signals inside or outside the stromal volume. To isolate the extra-stromal nerve signal, the corneal nerve intensity inside the stromal volume defined by the *Surface* tool was set to 0.0. Conversely, to isolate the intrastromal nerve signal, the signal intensity external to the stroma was set to 0.0. Separate channels for extra-stromal and intrastromal nerves were labeled in yellow and red, respectively. Then, using the *Filament* tool, the volumetric structure for the extra- and intrastromal corneal nerves was rendered. Finally, the statistical data were retrieved from the *Statistics* tab in Imaris, obtaining the volume parameter data from inside the *Detailed* section.

Neurotrophic Corneal Persistent Epithelial Defect Wound-Healing Model

To develop the neurotrophic corneal PED wound-healing model, corneal epithelial defects were physically created in C57BL/6 mice, and the cornea was treated or not with topical BAK administration. Briefly, mice were immobilized in a head holder and put under general anesthesia with isoflurane. The corneal surface was additionally anesthetized with 1% proparacaine hydrochloride ophthalmic eyedrops (Alcon, Fort Worth, TX, USA). The central 2 mm of the cornea was exposed to 20% ethanol for 30 seconds using a 2-mm circular trepan, then gently debrided with a blunt golf club spud held at approximately 45° from the corneal surface. In the BAK-treated group, 10 µL 0.1% BAK was instilled in the central cornea using a pipette. Ten seconds later, the corneal surface was rinsed four times with 2 mL PBS to prevent prolonged BAK exposure. In the untreated group, PBS was administrated instead of BAK. After creation of the corneal defect, fluorescein corneal staining and imaging were performed at 6-hour intervals for up to 24 hours.

To obtain in vivo corneal nerve images in the neurotrophic corneal PED model, CGRP:GFP Tg mice were used to induce corneal epithelial defects; corneal defects were created and treated or not with BAK, as described above. Measurement of corneal mechanosensation and in vivo multiphoton confocal microscopy (MCM) corneal imaging were performed at baseline (before defect creation) and 24 hours after epithelial defect creation. Fluorescein staining was not performed on these mice to avoid contamination of fluorescent signals when acquiring images with the in vivo MCM.

Correlation and Quantification of Persistent Epithelial Defect With Intravital Imaging

Imaging of corneal epithelial defects was performed under general anesthesia via isoflurane inhalation. The cornea was stained with 10 µL 0.5% fluorescein solution and immediately washed with PBS. The defects were then imaged under a microscope using a cobalt blue light filter. The obtained images were analyzed using Photoshop software (Adobe Inc., San Jose, CA, USA); the border of the corneal limbus and the epithelial defect border were manually traced. The area of the entire cornea, defined by the corneal limbus border, and that of the epithelial defect, defined by the epithelial defect border, were calculated by Photoshop and quantified in pixels. The relative area of epithelial defect was defined as the ratio of the absolute area of the defect to the absolute area of the entire corneal. Wound closure percentage at each time point was determined as follows[38]:

$$WCP_x\,(\%) = (A_o - A_X)\,/A_0 \times 100$$

WCP is the wound closure percentage, A_0 is the initial corneal epithelial defect area, and A_x is defect area at x hours after creating a corneal epithelial defect.

Corneal Esthesiometry Measurement

Corneal mechanosensation was measured with a Cochet–Bonnet esthesiometer (Western Ophthalmics, Lynwood, WA, USA) as previously described.[39] The filament was first applied in the central cornea at 60 mm (maximum length). Filament length was decreased by 5-mm increments and reapplied to the central cornea until a positive response, defined as reflexive blinking, was elicited. Measurements were obtained before (baseline) and 24 hours after the epithelial defect was created.

Quantitative Analysis of Corneal Nerves

Corneal nerves were imaged using in vivo MCM and analyzed by Imaris using the same method as described above. Nerve volumes using the analysis function of the Imaris software, the nerve volume (µm^3) and nerve length (µm), were obtained from each 3D-rendered corneal nerve image. Given the possibility of individual variation in absolute GFP intensity between each image, relative nerve volumes (%) and nerve lengths (%) were calculated with reference to baseline nerve volumes and then compared between each group.

Statistical Analysis

All data are presented as mean ± SD. Statistical analyses were performed using GraphPad Prism version 9.4.1 (GraphPad Software, San Diego, CA, USA). Statistical comparisons between wound closure percentage, corneal mechanosensation measurements, and corneal nerve volumes at baseline and 24 hours were made with the Mann–Whitney *U* test. A *P* value of <0.05 was considered statistically significant.

Results

In Vivo Characterization and Quantification of CGRP-Positive Corneal Nerve Axons Using MCM

First, as shown in Figure 1, using in vivo stereomicroscopic fluorescence microscopy of the cornea, CGRP-positive corneal axons were readily identified in green fluorescence in CGRP:GFP Tg mice. This method effectively reflects GFP expression as corneal nerves did not exhibit

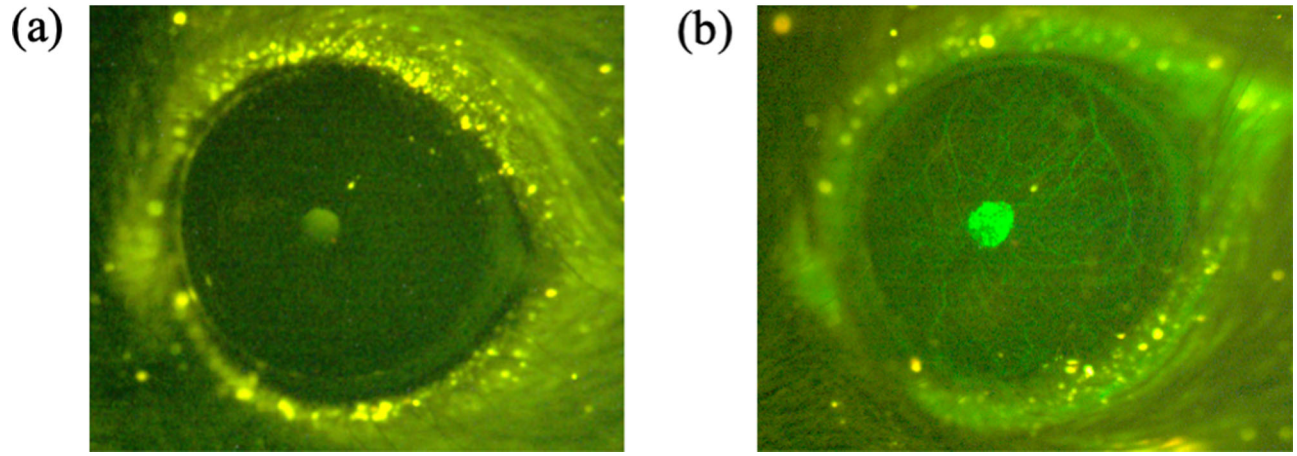

Figure 1. CGRP-positive nerves in CGRP:GFP Tg mouse imaged by fluorescence microscopy. Corneas of (**a**) wild-type (WT) and (**b**) CGRP:GFP Tg mice were imaged using fluorescence microscopy. CGRP-positive corneal nerves are visualized as bright green filaments only in the CGRP:GFP Tg mice. Corneal images obtained by fluorescence microscopy allow for in vivo visualization of the entire corneal nerve network.

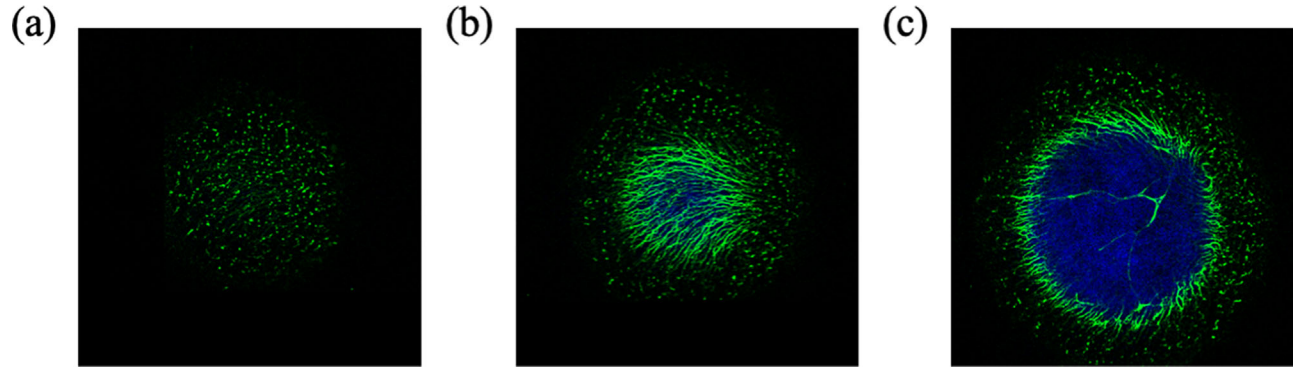

Figure 2. Slices of corneal images in CGRP:GFP Tg mice obtained by in vivo multiphoton confocal microscopy. Images obtained by in vivo multiphoton confocal microscopy depicted the unique distributions of the corneal nerves in CGRP:GFP Tg mice. (**a**) Terminals of intraepithelial nerve fibers were captured as numerous punctate signals (*green*) in the most superficial layer of the corneal epithelium. Within the epithelial layer, (**b**) nerves formed a dense meshwork, which represent the subbasal nerve plexus. (**c**) Nerves that appeared within the stroma (*blue*) were thicker than those in the epithelium and represented the subepithelial nerve plexus.

fluorescence in wild-type C57/B6 mice. These images depict the thick nerves in the corneal stroma as well as some of the thicker nerves in the epithelial layer but did not have enough resolution to capture the fine branches such as those extending terminally into the epithelial layer. This was due to the limitations of fluorescence microscopy, which involves more light scattering and has less resolution than confocal microscopy.

To improve the resolution of intravital microscopy, we employed MCM to capture the corneal nerves in 3D images in CGRP:GFP Tg mice with quantifiable elements and enhanced resolution, identifying distinct morphologic patterns at various depths in the cornea. In the raw in vivo MCM images, CGRP-positive nerves were clearly depicted by a green signal in every optical section (Fig. 2). These two-dimensional (2D) images depicted the unique distribution and morphology of corneal nerves that are characteristic of each layer of the cornea, from the superficial epithelium to the deeper stroma. In the superficial layer, numerous punctate signals were observed that likely represented intraepithelial nerve terminals. Immediately deep to the epithelium was a dense network of fine nerves representing the subbasal plexus. The CGRP-positive nerves within the corneal stroma appeared thicker but fewer in number and likely represented the subepithelial nerve plexus (Fig. 2).

While the collection of 2D optical sections clearly depicts CGRP-positive corneal nerves, the dome-like shape of the cornea limits observation of the overall distribution of GFP^+ nerves in 2D. Therefore, each series of corneal optical sections was processed in Imaris, which successfully yielded 3D reconstructions/images of CGRP-positive nerves (Fig. 3). These images provided valuable spatial information regarding nerve distribution relative to the stroma due to the unique potential for second harmonic–generated signals in MCM.

Classification of corneal nerves relative to the SHG signal of the stroma revealed unique networks of intrastromal (red) and extra-stromal (yellow) nerves. Intrastromal nerves predominantly contained thick nerves representing the subepithelial nerve plexus along with a meshwork of some of the thin nerves. In contrast, the extra-stromal epithe-

Investigative Ophthalmology & Visual Science

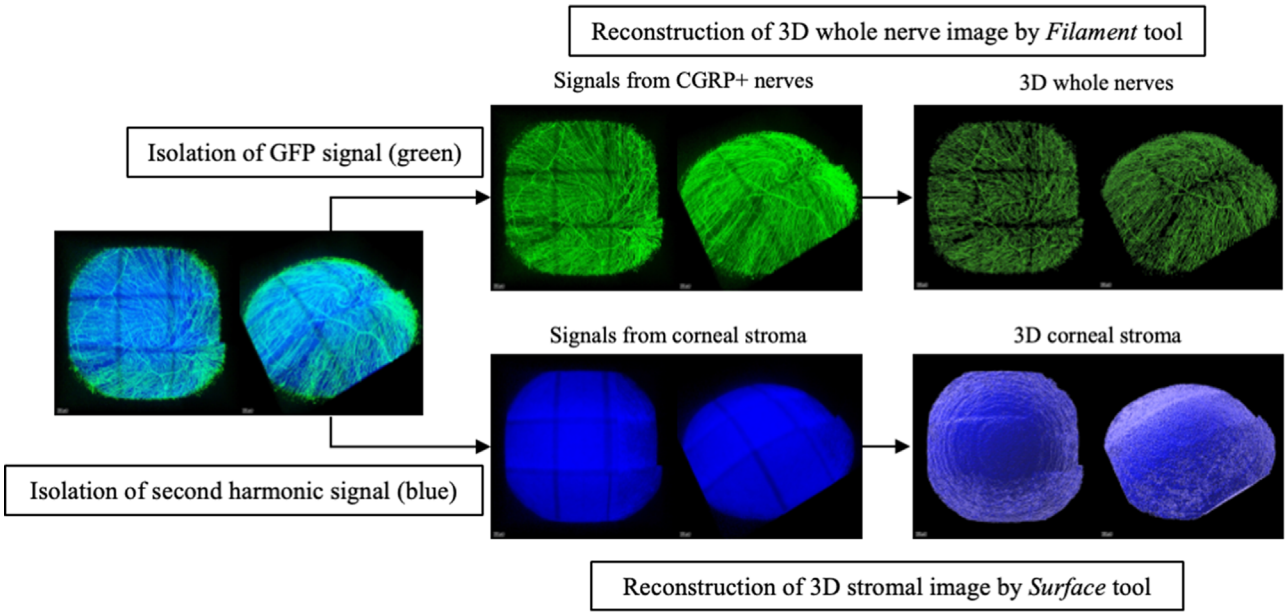

Figure 3. Reconstruction of 3D images of corneal nerves and stroma. GFP (*green*) signals and second harmonic signals (*blue*) from the corneal stroma in CGRP:GFP Tg mice were stitched and processed by image software Imaris. Green and blue signals were isolated from each other and then reconstructed into 3D images.

lial nerves predominantly contained the network of intraepithelial nerves and subepithelial nerve plexus. Thus, extrastromal nerves are interchangeably referred to as epithelial nerves in this study (Fig. 4a). The successful spatial classification of corneal nerves with respect to the stroma can elucidate the location of nerve damage in the corneal epithelial wound-healing model.

These 3D images allow for observation of corneal nerves from virtually any angle and magnification, providing a comprehensive overview of the corneal nerve topography (Fig. 4b) and detailed representations of fine structures (Figs. 4c, 4d). These virtual models can be manipulated in various ways, including viewing angles and image magnification, while also allowing for the analysis of quantitative parameters such as volume, surface area, and length of each nerve fiber using Imaris. Overall, the in vivo MCM and Imaris-based imaging system for murine corneal nerves in CGRP:GFP Tg mice was successfully developed and facilitated distinct visualization of the corneal nerves in live mice.

Delayed Corneal Epithelial Wound Healing Induced by Benzalkonium Chloride

In C57BL/6 mice, the progression of wound healing in the BAK-treated group (10 eyes of 10 mice) was compared to a control group (5 eyes of 5 mice) in which BAK was not applied for 10 seconds. The initial surface of the corneal lesion was comparable in the control group (47.8% ± 2.5% of the total cornea surface) and BAK group (50.4% ± 2.2%; $P = 0.1$). However, the time course of wound closure for each group revealed delayed onset of wound healing in the BAK group, which was evident 12 hours postprocedure. In the control group, the lesion almost entirely re-epithelialized by the 24-hour endpoint, whereas a complete epithelialization was not achieved in the BAK group (Figs. 5a, 5b). The wound closure percentage at the 24-hour endpoint was significantly lower in the BAK group compared to the control group (51.2% ± 13.3% vs. 96.9% ± 6.0%, respectively; $P = 0.0007$) (Fig. 5c). These results suggest that brief exposure to 0.1% BAK after corneal abrasion impairs the corneal epithelial wound-healing process and delays re-epithelialization.

Benzalkonium Chloride Induces Functional and Structural Damages on Corneal Nerves in the Delayed Corneal Epithelial Wound Healing

Corneal epithelial lesions were created in 12 eyes of six CGRP:GFP Tg mice, with 6 eyes treated with BAK and 6 eyes left untreated. Baseline corneal nerve images obtained before the procedure exhibited a similar distribution of the epithelial nerve plexus and network of thick stromal nerves in both groups.

The comparison of images taken 24 hours postprocedure showed that the epithelial nerve plexus disappeared in both groups, mainly in the central cornea (Fig. 6). A pronounced reduction of epithelial nerve length (19.0% ± 7.0% in control vs. 19.2% ± 9.2% in BAK-treated; $P > 0.99$) and volume (20.0% ± 11.2% in control vs. 16.0% ± 7.3% in BAK-treated; $P > 0.99$) compared to baseline was observed in both groups (Figs. 7a, 7b). These reductions in length and volume of epithelial nerves were attributable to the experimental corneal epithelial debridement. In the BAK group, the stromal nerve network was fragmented with a loss of continuity, whereas stromal nerves remained relatively preserved in the control group (Fig. 6). Regarding stromal nerves, although nerve length did not show a significant difference between both groups (44.3% ± 6.1% in control vs. 36.2% ± 14.7% in BAK-treated; $P = 0.352$), nerve volume was significantly decreased at 24 hours in the BAK group compared to the control group (49.4% ± 14.4% in control vs. 27.0% ± 11.0% in BAK-treated; $P = 0.019$) (Figs. 7a, 7b).

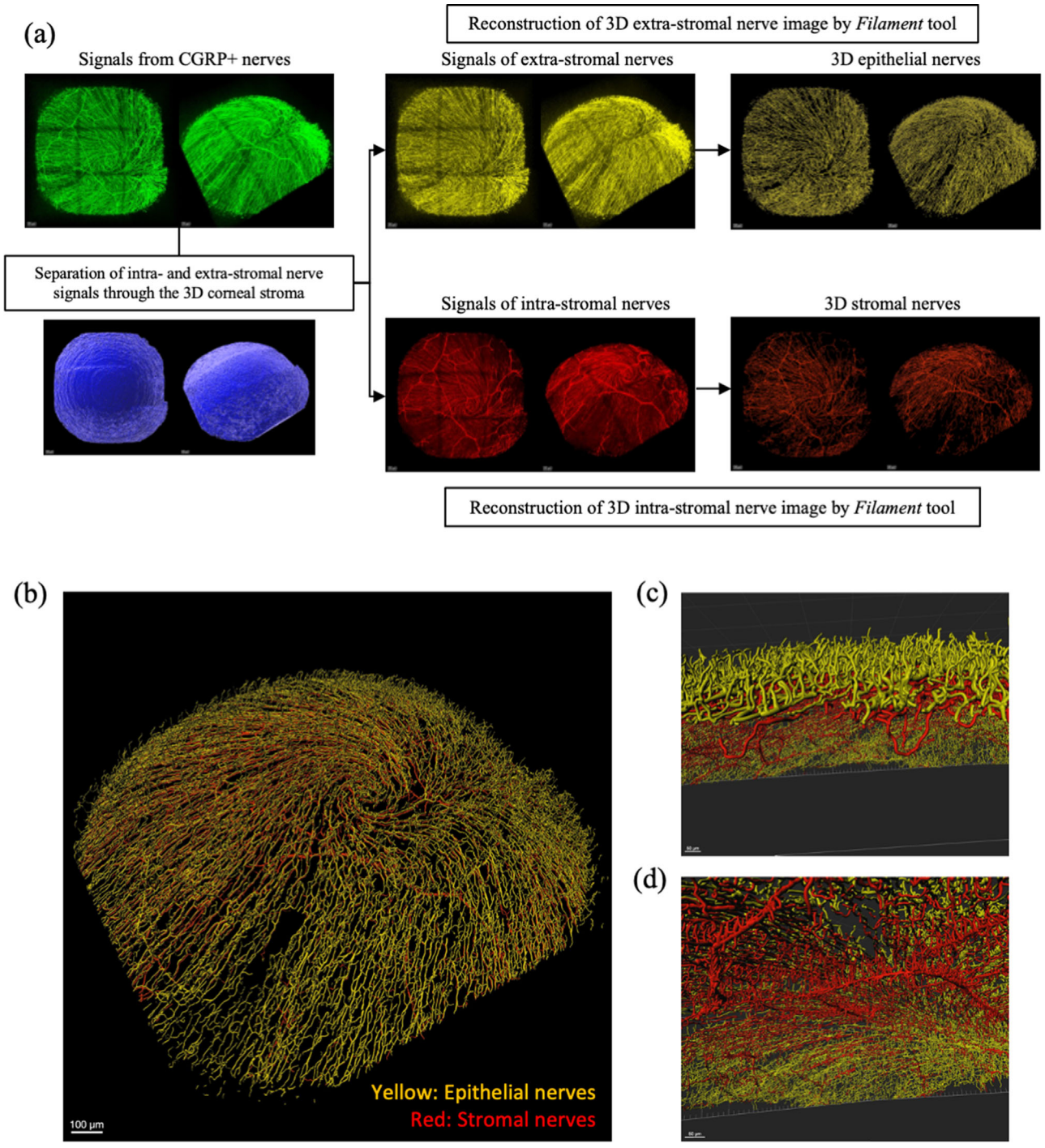

Figure 4. In vivo 3D image reconstruction of corneal nerves segmented into epithelial and parenchymal nerves based on corneal parenchymal signals. The 3D images of the CGRP-positive corneal nerves in CGRP:GFP Tg mice were successfully captured by in vivo multiphoton microscopy and processed by Imaris software. (**a**) Based on the 3D confines of corneal stroma revealed by its second harmonic–generated signal, GFP signals (*green*) were separated into two categories: extra-stromal (*yellow*: stromal nerves) and intrastromal (*red*: epithelial nerves) signals. Each category was then individually reconstructed into 3D images. In low magnification, the entire corneal nerve distribution can be observed. (**b**) Corneal epithelial nerves are distributed radially around the central corneal vortex, forming a subbasal nerve plexus. From a lateral view with high magnification, (**c**) the branches of epithelial nerves extending toward the corneal epithelium (intraepithelial terminals) are well represented. (**d**) Thick stromal nerves consisting of the subepithelial nerve plexus were identified from a posterior view.

These results suggest that BAK had a detrimental effect on stromal nerve damage after the intervention.

Functional analyses of corneal mechanosensation revealed no significant difference at baseline between wild-type and CGRP:GFP Tg mice (50.0 vs. 53.3 ± 0.41 mm) ($P = 0.2$). However, at 24 hours postprocedure, a significant decrease of mechanosensation was observed in the BAK group (25.0 ± 0.58 mm vs. 1.7 ± 2.6 mm) ($P = 0.0095$)

Investigative Ophthalmology & Visual Science

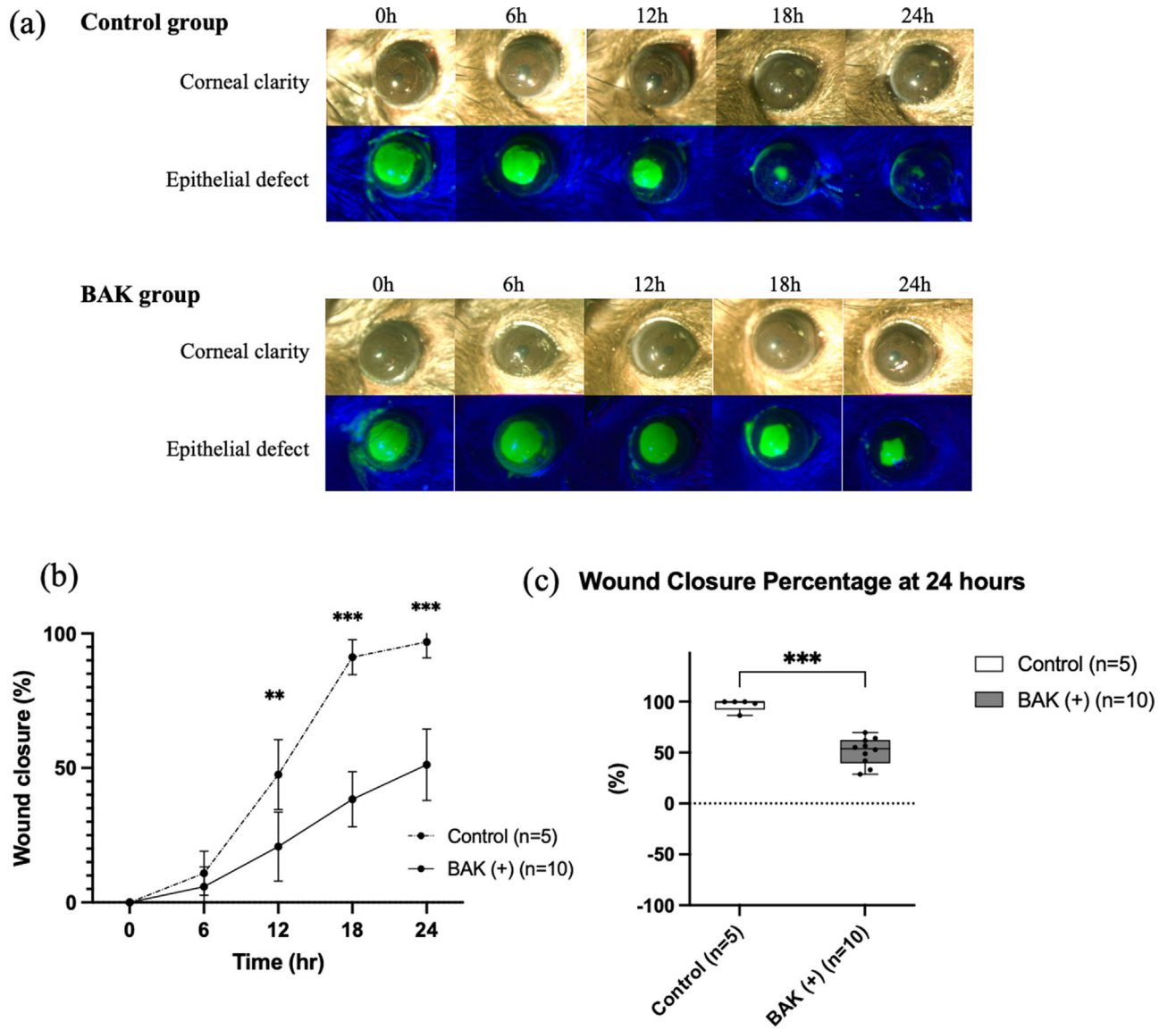

Figure 5. Delayed wound-healing process by benzalkonium chloride administration. Corneal epithelial defects were created with a 2-mm diameter and imaged with fluorescein staining using a blue-free filter every 6 hours, ranging from immediately after the creation of the defect up to 24 hours later. (**a**) Representative photos of cornea and corneal fluorescein staining showed that the control group showed quick and complete re-epithelialization at 24 hours while the BAK-treated group showed delayed wound healing and incomplete re-epithelialization at 24 hours. Wound closure percentage (WCP) was calculated as the percentage of area epithelialized over the baseline defect area. (**b**) Wound healing was significantly delayed in the BAK group compared to the control group at 12 hours after defect creation. (**c**) At 24 hours, the BAK group showed a significantly lower WCP than the control group ($P = 0.007$).

(Fig. 7c). These results indicate that BAK disrupted stromal nerve structure and impaired the corneal nerve function.

Discussion

There is a need for an in vivo model of neurotrophic corneal PEDs. In addition, there is also a need for a high-resolution and quantitative imaging modality that can provide visual data on corneal nerves in vivo. The combination of this model and imaging modality will facilitate investigating the pathophysiology of and therapeutics for diseases such as neurotrophic keratitis. This study presents both an effective murine model of neurotrophic corneal PEDs under specific treatment conditions as well as a method for in vivo visualization of corneal nerves in a transgenic mouse model.

In this study, we combined an in vivo MCM and CGRP:GFP Tg mice to visualize corneal nerves and obtain 3D images of them. This novel in vivo imaging technique allowed us to successfully observe corneal nerves over time to assess nerve damage in BAK-induced delayed corneal epithelial wound healing. Our mouse model recapitulates the pathophysiology of corneal epithelial defects in neurotrophic keratopathy, and it is ideal for this mouse model to use the CGRP:GFP Tg mice developed through the efforts of Bouheraoua et al.,[33] which allows us to focus on $CGRP^{+}$ nerves since they are peptidergic neurons involved in pain sensation,[7,33,40,41] and neuropeptides such as CGRP, substance P, and vasoactive intestinal peptide play a role in the corneal epithelial wound-healing process.[8,11,42,43]

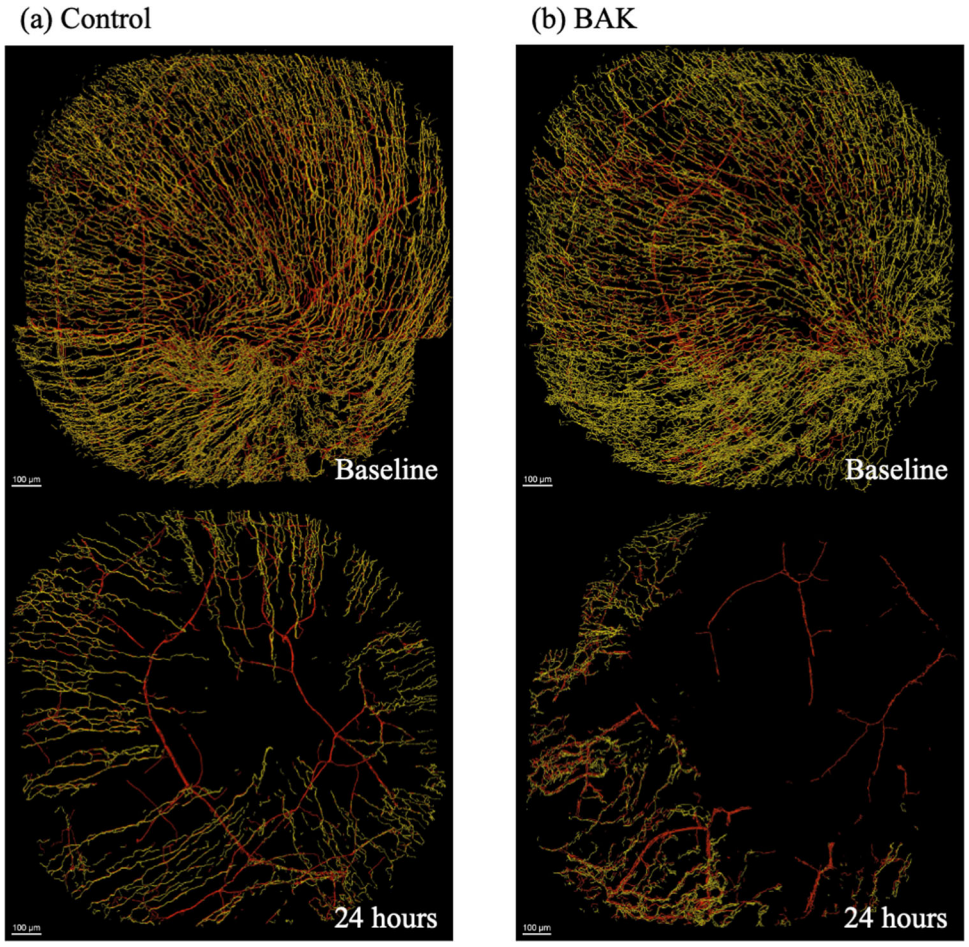

Figure 6. Destructive corneal epithelial and stromal nerve structures after corneal debridement and following benzalkonium chloride administration. The 3D models of corneal nerves in CGRP:GFP Tg mice were obtained by in vivo multiphoton microscopy and Imaris at baseline (*inset*) and 24 hours after corneal epithelial debridement. (**a**, **b**) Images show a drastic decrease in epithelial nerve volume (*yellow*), and the dense subbasal plexus virtually disappeared after corneal epithelial debridement in both the control and BAK groups. Stromal nerves (*red*) were fragmented and lost their continuity in (**b**) the BAK-applied eye, while the continuity of the stromal nerves was relatively preserved in (**a**) the control group.

The most important advantage provided by the combination of in vivo MCM and CGRP:GFP Tg mice is the ability to image the nociceptive axons in the cornea of live mice. This allows longitudinal analysis of corneal nerve structure, which is impossible with conventional histologic methods. Furthermore, a unique feature of multiphoton confocal microscopy is the ability to obtain second harmonic generation from the corneal stroma. It enables imaging of the corneal stroma without the need for any staining of the tissue or genetic modification for the expression of fluorescent proteins. Besides, the two-photon excitation is generally less scattered than one-photon excitation and therefore provides a higher resolution. The development of CGRP:GFP Tg mice also overcomes the possibility of incomplete immunohistochemical staining due to insufficient tissue penetration of antibodies. In fact, the GFP signals obtained in this study were sharp/strong enough to allow generating high-resolution 3D images of corneal innervation in a wide area and across its entire depth.

Regarding other in vivo microscopy techniques that visualize corneal nerves in mice, the use of confocal laser scanning microscopy, which has already been clinically applied in humans, has been reported to easily capture unlabeled corneal nerves.[27,44] Although corneal nerve mapping is a challenging process due to the small scanning area and the difficulty of repeatedly targeting precisely specified areas, various attempts have resulted in the successful delineation of a wide field of view of corneal innervation.[45–50] On the other hand, compared to the approach described herein, in vivo multiphoton confocal imaging far outperforms in terms of resolution, as confocal laser scanning microscopy cannot easily detect thin nerves such as intraepithelial terminals. Although fluorescence microscopy provides enough images to overview the entire corneal neural network, it was insufficient to visualize fine nerves, obtain detailed nerve distribution, or reconstruct 3D structures because it does not provide z-axis data. To summarize, the imaging system reported in this study using CGRP:GFP Tg mice and in vivo multiphoton confocal microscopy has a remarkable capability for repeated, noninvasive, longitudinal evaluation of corneal nerves with high resolution in mice, which allows for a comprehensive visualization of corneal innervation without the need of immunohistochemistry procedures.

It is necessary to carefully interpret the quantitative parameters obtained from the 3D imaging process. In this study, there was a discrepancy between the length and

Investigative Ophthalmology & Visual Science

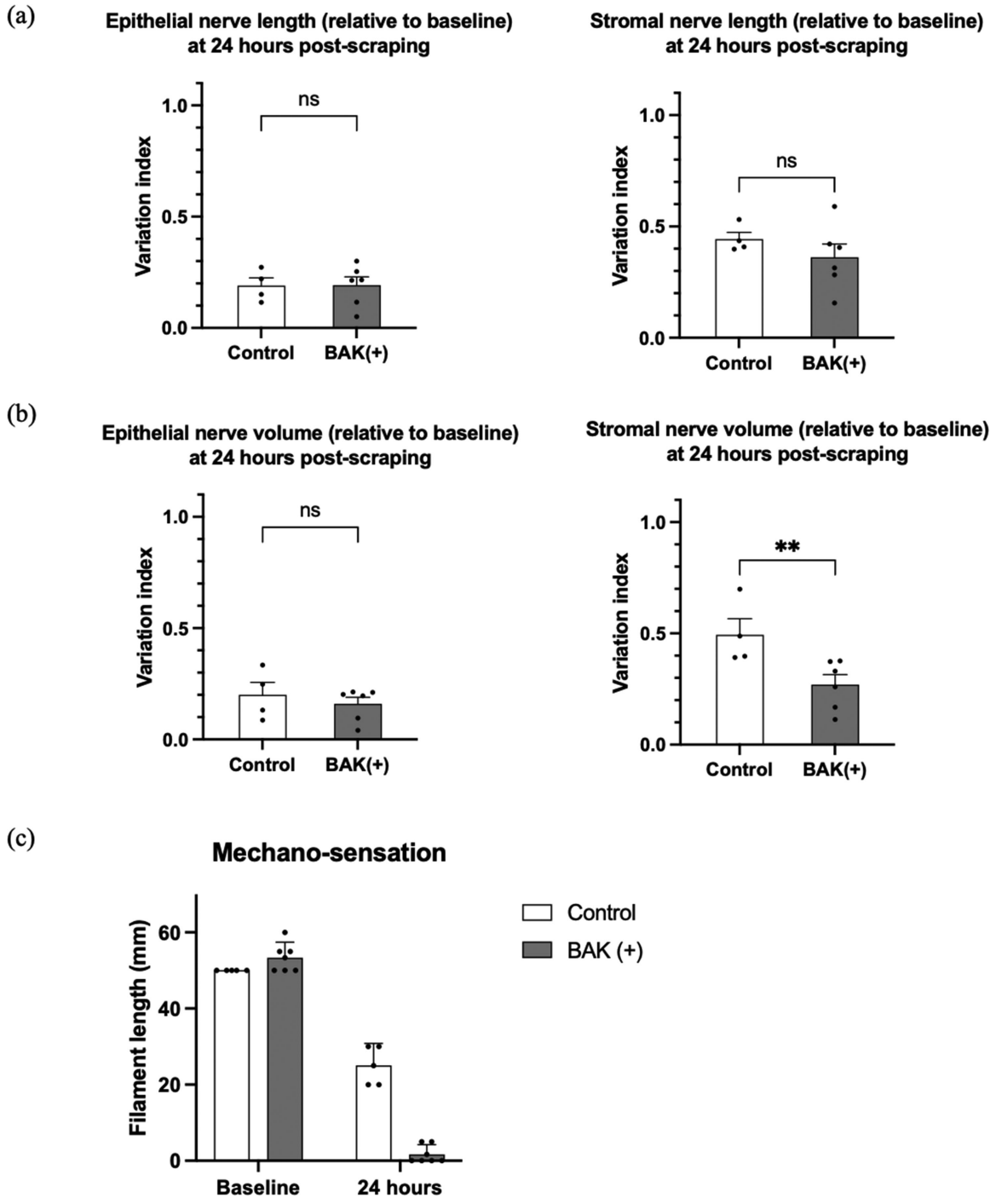

Figure 7. Corneal nerves were damaged both functionally and structurally by benzalkonium chloride. Corneal nerves were evaluated from both structural and functional perspectives. (**a**, **b**) Based on nerve lengths and volumes obtained in Imaris, the ratios of length and volume between baseline and 24-hour postprocedure of epithelial and stromal nerves were calculated. (**a**) Nerve length did not show significant differences between the BAK and control groups in both epithelial and stromal nerve length at 24 hours. (**b**) Although there was no significant difference between the BAK and control groups in epithelial nerve volume, stromal nerve volume at 24 hours was significantly ($P = 0.0095$) less in the BAK group than in the control group. (**c**) Corneal mechanosensation was measured using Cochett–Bonnet at baseline and 24 hours after corneal debridement. The BAK group showed significantly ($P = 0.0095$) impaired mechanosensation compared to the control group at 24 hours.

volume of the stromal nerves in the BAK and control groups. In the "filament" analysis process of Imaris software, the software recognized GFP signals as a series of points of varying size according to the intensity and reconstructed 3D nerve fibers by filling in the gaps. Therefore, reduction in GFP intensity or number of points directly affects the reconstructed nerve fiber's thickness and volume, as the fiber appears thinner. However, the length of fibers could be over-

estimated due to the modifications by the software in which gaps are filled in by the software, even when the signal count or intensity is reduced. Consequently, fiber length alone may not fully capture changes in GFP signal intensity or volume. In addition, after surgical intervention, morphologic changes in the nerve, such as swelling of the nerve axon, may affect nerve diameter and thus volume measurements. However, the CGRP-GFP transgenic mice used in this study express GFP, which labels the neurotransmitter CGRP, rather than directly labeling nerve fibers or axonal structures. While GFP enables visualization of CGRP-positive pathways, it represents changes in the localization and amount of CGRP, not the structural nerve alterations themselves. Therefore, the intensity and number of GFP signals reflect CGRP levels, indicating changes in neurotransmitter presence rather than nerve fiber morphology. Through this indirect analysis, we observed neuronal pathway changes as fluctuations in CGRP expression rather than direct structural modifications of the neural tissue. Therefore, it should be noted that both length and volume aspects require to be comprehensively interpreted.

In the present study, the volume of stromal nerves was significantly decreased in the BAK group compared to the control group, while there was no significant difference in the length of nerve fibers between the two groups. According to these results, GFP signals were reduced and/or weakened, suggesting that functional changes, such as CGRP production and transport, were impaired. On the other hand, it could be understood that there was no significant difference in the extent of structural destruction of the nerve fibers, at least for the total length of the nerve, suggesting that the pathways of CGRP-positive nerves may have been maintained at the same level in the two groups. It is therefore considered that the results of this study emphasize impairment of neurotransmitter activity rather than the physical integrity of the neural pathways.

Herein we describe a novel mouse model for investigating BAK-induced delayed corneal epithelial wound healing. Although our model of BAK-induced keratopathy may not fully represent the pathophysiology of neurotrophic keratopathy (NK), patients using glaucoma medications containing BAK are known to develop decreased corneal sensitivity and "NK"-like keratopathy.[51] The mechanism of BAK damage to corneal epithelial cells has been well investigated, as it involves such factors as cytotoxicity, oxidative stress/reactive oxygen species production, inhibition of metabolic activity, membrane permeability, induction of apoptosis, and production of inflammatory cytokines.[17–23] It has been documented that BAK induces neurotoxicity directly by its detergent effect and indirectly by its infiltration of inflammatory cells and promotion of inflammation.[24–28,52] Several reports evaluate the effect of BAK on corneal epithelial wound healing in mice, and all of them reported that BAK causes a delay in corneal epithelial wound healing.[15,16] The delayed corneal epithelial wound healing and neuronal damage observed in our study should also be caused by those previously described mechanisms. In addition, it should be considered there was a possibility that poor wound healing could also be affected by BAK toxicity to limbal stem cells. In our model, it is important to note that the corneal epithelium was intentionally debrided and BAK was administered at a concentration more than five times higher than the usual ophthalmic formulation. Although the multilayered structure and tight junctions of the corneal epithelium provide barrier function,[53] the lack of the barrier resulted in the toxicity of BAK directly affecting the basement membrane, stroma, and nerves. Therefore, it was considered that the corneal wound healing and nerves were damaged even though the exposure to BAK was only once for 10 seconds. Our model allows for testing other therapeutic agents without concern for any interference such as dilution, washout, or interaction with BAK due to repetitive BAK administration. This is an advantage of our model for evaluating treatment efficacy in delayed corneal wound healing.

Corneal mechanosensation was dramatically reduced in eyes exposed to BAK or not, a phenomenon likely explained by the loss of epithelial nerve terminals after epithelial debridement. In an intact cornea, numerous intraepithelial terminals extend from the subbasal plexus to the epithelial layer, providing exquisite sensation to this organ.[1] Since stimulus sensing begins with the activation of receptors present in nerve terminals, the loss of intraepithelial nerve endings by scraping could lead to a dramatic decrease in mechanosensation. Interestingly, corneal mechanosensation was significantly lower and almost abolished in the BAK group compared to the control group. Several possible mechanisms might underlie the differences in corneal mechanosensation between the BAK and control groups. As can be seen from the in vivo nerve images, most of the intraepithelial nerves were lost in the central cornea after epithelial defect creation. This finding is consistent with the dramatic decrease in nerve volume in both groups. However, focusing on the overall distribution of epithelial nerves, epithelial nerves grew toward the center of the cornea in the control group over time, whereas large areas without epithelial nerves in the center of the cornea persisted in the BAK group. This suggests that the decreased number of epithelial nerves growing toward the center of the cornea may contribute to impaired mechanosensation.

Another possible explanation is that the stromal nerves partially contribute to mechanical sensation, as suggested by the clear difference in the morphology of stromal nerves between both groups. Receptors of corneal nerves are considered located almost entirely at the epithelial nerve endings,[40] while the presence of receptors deeper than the epithelium layer in the central cornea has not been clarified. However, the presence of nerve-end bulbs, called corpuscular nerve endings, has been reported in the corneal limbus and conjunctiva.[54,55] There is a possibility that there may be unknown sensory receptors in the corneal stroma, in the same way that there are various sensory receptors in different layers of epidermis and dermis.[56] Given these considerations, it is not surprising if sensory receptors exist in corneal stroma, and our results may reflect the possible function of these hypothetical sensory receptors. Of course, since this study focused only on CGRP-positive nerves, which are polymodal fibers, it is possible that other CGRP-negative nerves, such as pure mechanical sensory nerves, are involved in mechanosensation and remained after removal of the corneal epithelium.

Although further research is needed to elucidate the mechanism of perception of mechanical stimulation in the cornea lacking corneal epithelium, our results suggest that BAK administration may have triggered damage to the neural structure and receptor function of the stromal layer. Therefore, BAK application might delay corneal epithelial wound healing by damaging both the corneal epithelium and the corneal nerves. In addition, while there is no doubt that an impairment of corneal axons was caused by BAK

Investigative Ophthalmology & Visual Science

administration, the reduction of corneal nerve volume could also reflect a decrease in CGRP or GFP expression. Therefore, further studies are needed to elucidate the underlying pathophysiology, such as structural destruction of neurons and axons or impairment of functions such as neuropeptide production, distribution, and transport.

In summary, we successfully observed corneal nociceptive nerves longitudinally using CGRP:GFP Tg mice and in vivo multiphoton confocal microscopy. Combining our wound-healing model with a novel imaging system enabled us to evaluate structural and functional changes in corneal nerves longitudinally in conjunction with assessing wound healing through conventional methods. This experimental system offers outstanding potential for various applications and will contribute to the detailed investigation of neurotrophic persistent epithelial defects and the development of new therapeutic approaches.

Acknowledgments

The authors thank Jose Echegarray and Liwen Lin for their expert assistance with lab management and animal care.

Supported by NIH/NEI R01EY030283 (VLP), NIH/NEI R01EY024484 (VLP), Duke NIH Center Core Grant P30EY005722 (VLP), NEI U1 Grant U01EY034687 (VLP), and Duke Research to Prevent Blindness Unrestricted Grant (VLP).

Disclosure: **S. Komai**, None; **M.E. Quiroga-Garza**, None; **R.E. Ruiz-Lozano**, None; **N.S. Azar**, None; **H.M. Mousa**, None; **S. Murillo**, None; **S. Ma**, None; **A. Khodor**, None; **S. Littleton**, None; **D.R. Saban**, None; **A. Chédotal**, None; **V.L. Perez**, Brill Pharma (C), BRIM Pharma (C), Claris Biotherapeutics (C), Dompé (C), Kala (C), Nicox (C), Thea (C), Trefoil (C), NEI/NIH (F), Claris Biotherapeutics (I), Eniale Immunotherapeutics (I), Trefoil (I)

References

1. Ruiz-Lozano RE, Hernandez-Camarena JC, Loya-Garcia D, Merayo-Lloves J, Rodriguez-Garcia A. The molecular basis of neurotrophic keratopathy: diagnostic and therapeutic implications. A review. *Ocular Surface*. 2021;19:224–240.
2. Suzuki K, Saito J, Yanai R, et al. Cell-matrix and cell-cell interactions during corneal epithelial wound healing. *Prog Retin Eye Res*. 2003;22:113–133.
3. Dua HS, Said DG, Messmer EM, et al. Neurotrophic keratopathy. *Prog Retin Eye Res*. 2018;66:107–131.
4. Malhotra R, Elalfy MS, Kannan R, Nduka C, Hamada S. Update on corneal neurotisation. *Br J Ophthalmol*. 2019;103:26–35.
5. Soni NG, Jeng BH. Blood-derived topical therapy for ocular surface diseases. *Br J Ophthalmol*. 2016;100:22–27.
6. Vajpayee RB, Thomas S, Sharma N, Dada T, Tabin GC. Large-diameter lamellar keratoplasty in severe ocular alkali burns: a technique of stem cell transplantation. *Ophthalmology*. 2000;107:1765–1768.
7. Belmonte C, Acosta MC, Gallar J. Neural basis of sensation in intact and injured corneas. *Exp Eye Res*. 2004;78:513–525.
8. Nakamura M, Kawahara M, Morishige N, Chikama T, Nakata K, Nishida T. Promotion of corneal epithelial wound healing in diabetic rats by the combination of a substance P-derived peptide (FGLM-NH2) and insulin-like growth factor-1. *Diabetologia*. 2003;46:839–842.
9. Wan L, Bai X, Zhou Q, et al. The advanced glycation end-products (AGEs)/ROS/NLRP3 inflammasome axis contributes to delayed diabetic corneal wound healing and nerve regeneration. *Int J Biol Sci*. 2022;18:809–825.
10. Wang Y, Wan L, Zhang Z, Li J, Qu M, Zhou Q. Topical calcitriol application promotes diabetic corneal wound healing and reinnervation through inhibiting NLRP3 inflammasome activation. *Exp Eye Res*. 2021;209:108668.
11. Zhang Y, Gao N, Wu L, et al. Role of VIP and sonic hedgehog signaling pathways in mediating epithelial wound healing, sensory nerve regeneration, and their defects in diabetic corneas. *Diabetes*. 2020;69:1549–1561.
12. Vaidyanathan U, Hopping GC, Liu HY, et al. Persistent corneal epithelial defects: a review article. *Med Hypothesis Discov Innov Ophthalmol*. 2019;8:163–176.
13. Vera-Duarte GR, Jimenez-Collado D, Kahuam-López N, et al. Neurotrophic keratopathy: general features and new therapies. *Surv Ophthalmol*. 2024;69:789–804.
14. Lin Z, Liu X, Zhou T, et al. A mouse dry eye model induced by topical administration of benzalkonium chloride. *Mol Vis*. 2011;17:257–264.
15. Nagai N, Murao T, Okamoto N, Ito Y. Comparison of corneal wound healing rates after instillation of commercially available latanoprost and travoprost in rat debrided corneal epithelium. *J Oleo Sci*. 2010;59:135–141.
16. Seino S, Matsuoka R, Masuda Y, Kunou M, Okada Y, Saika S. Topical hyaluronan alone promotes corneal epithelial cell migration whereas combination with benzalkonium chloride impairs epithelial wound healing. *Cutan Ocul Toxicol*. 2020;39:13–20.
17. Pauly A, Roubeix C, Liang H, Brignole-Baudouin F, Baudouin C. In vitro and in vivo comparative toxicological study of a new preservative-free latanoprost formulation. *Invest Ophthalmol Vis Sci*. 2012;53:8172–8180.
18. Smedowski A, Paterno JJ, Toropainen E, Sinha D, Wylegala E, Kaarniranta K. Excipients of preservative-free latanoprost induced inflammatory response and cytotoxicity in immortalized human HCE-2 corneal epithelial cells. *J Biochem Pharmacol Res*. 2014;2:175–184.
19. Soriano-Romaní L, García-Posadas L, López-García A, Paraoan L, Diebold Y. Thrombospondin-1 induces differential response in human corneal and conjunctival epithelial cells lines under in vitro inflammatory and apoptotic conditions. *Exp Eye Res*. 2015;134:1–14.
20. Tsai TY, Chen TC, Wang IJ, et al. The effect of resveratrol on protecting corneal epithelial cells from cytotoxicity caused by moxifloxacin and benzalkonium chloride. *Invest Ophthalmol Vis Sci*. 2015;56:1575–1584.
21. Vitoux MA, Kessal K, Melik Parsadaniantz S, et al. Benzalkonium chloride-induced direct and indirect toxicity on corneal epithelial and trigeminal neuronal cells: proinflammatory and apoptotic responses in vitro. *Toxicol Lett*. 2020;319:74–84.
22. Wu H, Zhang H, Wang C, et al. Genoprotective effect of hyaluronic acid against benzalkonium chloride-induced DNA damage in human corneal epithelial cells. *Mol Vis*. 2011;17:3364–3370.
23. Xu M, Sivak JG, McCanna DJ. Comparison of the effects of ophthalmic solutions on human corneal epithelial cells using fluorescent dyes. *J Ocul Pharmacol Ther*. 2013;29:794–802.
24. Chen W, Zhang Z, Hu J, et al. Changes in rabbit corneal innervation induced by the topical application of benzalkonium chloride. *Cornea*. 2013;32:1599–1606.
25. Gomes JAP, Azar DT, Baudouin C, et al. TFOS DEWS II iatrogenic report. *Ocular surface*. 2017;15:511–538.
26. Ivanusic JJ, Wood RJ, Brock JA. Sensory and sympathetic innervation of the mouse and guinea pig corneal epithelium. *J Comp Neurol*. 2013;521:877–893.

27. Martone G, Frezzotti P, Tosi GM, et al. An in vivo confocal microscopy analysis of effects of topical antiglaucoma therapy with preservative on corneal innervation and morphology. *Am J Ophthalmol*. 2009;147:725–735.e721.
28. Sarkar J, Chaudhary S, Namavari A, et al. Corneal neurotoxicity due to topical benzalkonium chloride. *Invest Ophthalmol Vis Sci*. 2012;53:1792–1802.
29. Alamri A, Bron R, Brock JA, Ivanusic JJ. Transient receptor potential cation channel subfamily V member 1 expressing corneal sensory neurons can be subdivided into at least three subpopulations. *Front Neuroanat*. 2015;9:71.
30. Marfurt CF, Murphy CJ, Florczak JL. Morphology and neurochemistry of canine corneal innervation. *Invest Ophthalmol Vis Sci*. 2001;42:2242–2251.
31. Murata Y, Masuko S. Peripheral and central distribution of TRPV1, substance P and CGRP of rat corneal neurons. *Brain Res*. 2006;1085:87–94.
32. Shimizu T, Toriumi H, Sato H, et al. Distribution and origin of TRPV1 receptor-containing nerve fibers in the dura mater of rat. *Brain Res*. 2007;1173:84–91.
33. Bouheraoua N, Fouquet S, Marcos-Almaraz MT, Karagogeos D, Laroche L, Chédotal A. Genetic analysis of the organization, development, and plasticity of corneal innervation in mice. *J Neurosci*. 2019;39:1150–1168.
34. Taurone S, Miglietta S, Spoletini M, et al. Age related changes seen in human cornea in formalin fixed sections and on biomicroscopy in living subjects: a comparison. *Clin Anat*. 2020;33:245–256.
35. Sawaguchi S, Fukuchi T, Abe H, Kaiya T, Sugar J, Yue BY. Three-dimensional scanning electron microscopic study of keratoconus corneas. *Arch Ophthalmol (Chicago, Ill: 1960)*. 1998;116:62–68.
36. Courson JA, Smith I, Do T, et al. Serial block-face scanning electron microscopy reveals neuronal-epithelial cell fusion in the mouse cornea. *PLoS One*. 2019;14:e0224434.
37. Jamali A, Seyed-Razavi Y, Chao C, et al. Intravital multiphoton microscopy of the ocular surface: alterations in conventional dendritic cell morphology and kinetics in dry eye disease. *Front Immunol*. 2020;11:742.
38. Abdel-Naby W, Cole B, Liu A, et al. Treatment with solubilized silk-derived protein (SDP) enhances rabbit corneal epithelial wound healing. *PLoS One*. 2017;12:e0188154.
39. Chucair-Elliott AJ, Zheng M, Carr DJ. Degeneration and regeneration of corneal nerves in response to HSV-1 infection. *Invest Ophthalmol Vis Sci*. 2015;56:1097–1107.
40. Belmonte C, Acosta MC, Merayo-Lloves J, Gallar J. What causes eye pain? *Curr Ophthalmol Rep*. 2015;3:111–121.
41. Quiroga-Garza ME, Ruiz-Lozano RE, Azar NS, et al. Noxious effects of riot control agents on the ocular surface: pathogenic mechanisms and management. *Front Toxicol*. 2023;5:1118731.
42. Mikulec AA, Tanelian DL. CGRP increases the rate of corneal re-epithelialization in an in vitro whole mount preparation. *J Ocul Pharmacol Ther*. 1996;12:417–423.
43. Tuncel N, Yildirim N, Gurer F, et al. Effect of vasoactive intestinal peptide on the wound healing of alkali-burned corneas. *Int J Ophthalmol*. 2016;9:204–210.
44. Reichard M, Hovakimyan M, Guthoff RF, Stachs O. In vivo visualisation of murine corneal nerve fibre regeneration in response to ciliary neurotrophic factor. *Exp Eye Res*. 2014;120:20–27.
45. Allgeier S, Bartschat A, Bohn S, et al. Real-time large-area imaging of the corneal subbasal nerve plexus. *Sci Rep*. 2022;12:2481.
46. Allgeier S, Bartschat A, Bohn S, et al. 3D confocal laser-scanning microscopy for large-area imaging of the corneal subbasal nerve plexus. *Sci Rep*. 2018;8:7468.
47. Allgeier S, Maier S, Mikut R, et al. Mosaicking the subbasal nerve plexus by guided eye movements. *Invest Ophthalmol Vis Sci*. 2014;55:6082–6089.
48. Edwards K, Pritchard N, Gosschalk K, et al. Wide-field assessment of the human corneal subbasal nerve plexus in diabetic neuropathy using a novel mapping technique. *Cornea*. 2012;31:1078–1082.
49. Lum E, Golebiowski B, Swarbrick HA. Mapping the corneal sub-basal nerve plexus in orthokeratology lens wear using in vivo laser scanning confocal microscopy. *Invest Ophthalmol Vis Sci*. 2012;53:1803–1809.
50. Turuwhenua JT, Patel DV, McGhee CN. Fully automated montaging of laser scanning in vivo confocal microscopy images of the human corneal subbasal nerve plexus. *Invest Ophthalmol Vis Sci*. 2012;53:2235–2242.
51. Villalba M, Sabates V, Orgul S, Perez VL, Swaminathan SS, Sabater AL. Detection of subclinical neurotrophic keratopathy by noncontact esthesiometry. *Ophthalmol Ther*. 2024;13:2393–2404.
52. Ivakhnitskaia E, Souboch V, Dallacasagrande V, et al. Benzalkonium chloride, a common ophthalmic preservative, compromises rat corneal cold sensitive nerve activity. *Ocular Surface*. 2022;26:88–96.
53. Sugrue SP, Zieske JD. ZO1 in corneal epithelium: association to the zonula occludens and adherens junctions. *Exp Eye Res*. 1997;64:11–20.
54. Lawrenson JG, Ruskell GL. The structure of corpuscular nerve endings in the limbal conjunctiva of the human eye. *J Anat*. 1991;177:75–84.
55. Al-Aqaba MA, Dhillon VK, Mohammed I, Said DG, Dua HS. Corneal nerves in health and disease. *Prog Retin Eye Res*. 2019;73:100762.
56. Abraira VE, Ginty DD. The sensory neurons of touch. *Neuron*. 2013;79:618–639.

Investigative Ophthalmology & Visual Science